

VERIFICATION OF DISLOCATION DENSITY AND DYNAMIC RECRYSTALLIZATION IN DEFORMED PURE COPPER

S. H. Huang,^{a,b,1} T. Chen,^c Q. Chen,^a Z. D. Zhao,^{a,b}

UDC 539.4

X. S. Xia,^a and Y. Wu^a

The mechanisms of dynamic recovery and dynamic recrystallization significantly affect the mechanical behavior and microstructure of the materials deformed at high temperatures. The modified Kocks and Mecking (K–M) model was used to assess the evolution of dislocation density of pure copper under high-temperature compression. The relationship between the deformation conditions and model parameters was derived and verified. The model offers quantitative prediction of flow stress curves, a recrystallized fraction, and recrystallized grain size under different conditions. The model can well integrate the recrystallization mechanism during deformation. The dislocation density and dynamic recrystallization evolution of pure copper provide a basis for optimizing thermomechanical processing in different fields of industry.

Keywords: pure copper, dislocation density, constitutive model, dynamic recrystallization, grain size.

Introduction. Thermomechanical plastic deformation behavior of metallic materials has integrated the advantages of controlling their geometry and microstructure. The constitutive model is important in the design and simulation of product-forming process and can reflect the evolution of stresses and strains. Dynamic recovery (DRV) and dynamic recrystallization (DRX) are important mechanisms for improving the performance of products, since microstructure of materials is closely related to their dislocation evolution. Complex types of mechanical behavior and microstructure are caused by the concurrent effects of work-hardening (WH), secondary work hardening (SWH), DRV, and DRX during hot deformation. Therefore, dislocation evolution is important for the hot deformation of metallic materials.

In the thermoplastic compressive deformation process of metal materials, stresses firstly increase with strains and then reach their peak values [1–5]. After that, the stress has several possible changing patterns. Firstly, the stress is maintained at the same level, due to the effect of DRV, or fluctuates. Secondly, the stress decreases gradually, due to the effect of DRX. Thirdly, due to the effect of SWH, the stress increases gradually again after the steady state strain is achieved. The DRX steady state is the equilibrium state between DRX softening and WH. After the DRX steady state is realized in the hot deformation process, the steady flow stress and average grain size is achieved. The DRX steady-state behavior of pure copper in the hot deformation process was explored, and the DRX grain size was found to be inversely proportional to flow stress under the steady state with an exponent of 1/2 [6].

The relationship between thermomechanical parameters and the strain hardening and softening kinetics had been extensively explored through some models, especially the Arrhenius hyperbolic-sine equation. The constitutive equations constructed by Sun et al. [7] precisely predicted the peak stress of the Mg–xZn–yEr alloys. Li et al. [8] constructed a constitutive model and explored the effects of strain, deformation temperature and strain rate on the

^aSouthwest Technology and Engineering Research Institute, Chongqing, China (¹hsh82@163.com).

^bPrecision Forming Integrated Manufacturing Technology of Collaborative Innovation Center, Chongqing, China.

^cInner Mongolia Dynamic and Mechanical Institute, Inner Mongolia, China. Translated from Problemy Prochnosti, No. 1, pp. 23 – 30, January – February, 2020. Original article submitted July 17, 2019.

yield stress of Al–Cu–Li–Sc–Zr alloy. The Kocks and Mecking (K–M) model [9–14] was used to analyze the evolution of dislocation density. In this K–M model, the microstructural evolution was described with the dislocation density. Huang et al. [10] explored the evolution of the dislocation density of 5754 aluminum alloy by K–M type plots. However, the prediction of the dislocation density evolution of pure copper in DRV, DRX, and SWH processes was seldom reported.

In this study, a refined K–M model of dislocation density evolution was established. The stress-strain data of pure copper were compared and verified to investigate the dislocation and stress evolution rules (WH, DRV, DRX, and SWH) under high-temperature compressive deformation. In addition, based on the dislocation evolution, the metallographic structure, and the DRX mechanism, the effects of temperature and strain rate on the grain size were analyzed.

1. Model Description. The modified K–M model [10] is provided as follows:

$$\frac{\partial \rho}{\partial \varepsilon} = k_1 \sqrt{\rho} - k_2 \rho, \quad (1)$$

where the multiplication term $k_1 \sqrt{\rho}$ indicates the accumulated moving dislocation density, the annihilation term $k_2 \rho$ denotes the dislocation annihilation during dynamic softening, while k_1 and k_2 values are correlated with the strain.

The dislocation density-flow stress relationship is expressed as [14, 15]

$$\sigma = \alpha \mu b \sqrt{\rho}, \quad (2)$$

where α denotes the Taylor constant, μ represents the shear modulus, and b is the Burgers vector.

The stress is correlated with the strain under the same conditions of temperature and strain rate. Equations (1) and (2) can be deduced as

$$\frac{\partial \rho}{\partial \varepsilon} = \frac{2\sigma\theta}{(a\mu b)^2}, \quad (3)$$

$$k_1 = \frac{2\theta\sigma_{sat}}{a\mu b(\sigma_{sat} - \sigma)}, \quad (4)$$

$$k_2 = \frac{2\theta}{\sigma_{sat} - \sigma}, \quad (5)$$

where σ_{sat} is the saturation stress, $\sigma_{sat} = \alpha \mu b \sqrt{\rho_{sat}}$, ρ_{sat} is the dislocation density of saturation state, and θ is the current work-hardening rate, $\theta = \partial \sigma / \partial \varepsilon$. Assuming that the entire deformation time t_{total} from the initial deformation ε_0 to the cumulative true strain ε_{total} is evenly subdivided into N deformation periods with a time step Δt , coefficients k_{1i} and k_{2i} in each deformation period can be respectively approximated as constants. When the strain rate $\dot{\varepsilon}$ is constant, the yield stress σ_i of the i th deformation period is derived as

$$\sigma_i = \sigma_{sat} - (\sigma_{sat} - \sigma_{i-1}) \exp\left(-\frac{k_{2i}}{2}(\varepsilon_i - \varepsilon_{i-1})\right). \quad (6)$$

2. Experimental Results and Discussion. In the simulation, the compressive deformation process of pure copper at high temperatures is subdivided into N deformation periods. The time step of each deformation period is Δt , and the product of the design time step Δt and the strain rate $\dot{\varepsilon}$ is 0.002, i.e., $\dot{\varepsilon} \Delta t = 0.002$. Then, the equivalent strain of the i th deformation period $\varepsilon_i = 0.002i$. At 700°C, under the strain rates of 0.001 and 0.01 s⁻¹, the stress

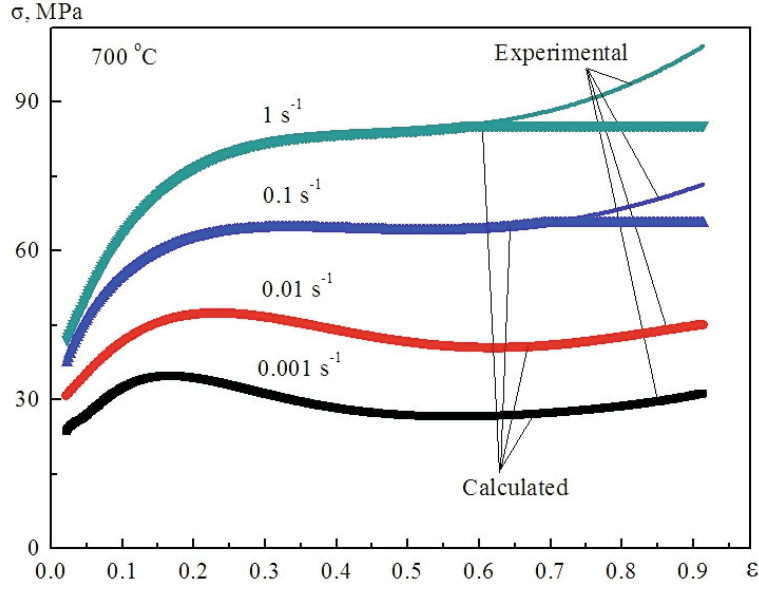


Fig. 1. Stress–strain curves of pure copper under different strain rates and 700°C.

decreases gradually when the DRX softening effect occurs (Fig. 1). Under the strain rates of 0.1 and 1 s^{-1} , the main deformation mechanism is the DRV. When the SWH occurs, the stress increases gradually. Figure 1 shows the comparison between the stress calculated by Eq. (6) and the experimentally obtained stress. Under the strain rates of 0.001 and 0.01 s^{-1} , the calculated stress basically coincides with the experimentally obtained stress, and the corresponding stress–strain curves are superposed. Under the strain rates of 0.1 and 1 s^{-1} , when the stress is lower than the saturated stress, the calculated stress–strain curves are superposed to the experimental stress–strain curves. When the stress is higher than the saturation stress, the calculated stress–strain curve remains stable indicating that Eq. (6) cannot describe the deformation mechanism of SWH.

When the SWH stress is higher than the saturation stress, in order to better describe the deformation mechanism of SWH, the saturation stress in Eq. (6) is substituted by the maximum stress. Then, evolutions of the coefficient k_2 with strain ε are calculated (Fig. 2). The coefficient k_2 varies with strain, indicating the relationship between the strain-hardening rate θ and the stress σ . The stresses calculated with different strain rates are consistent with the experimentally obtained stresses, and all stress–strain curves coincide with each other, indicating that the deformation mechanisms of DRV, DRX, and SWH can be well reflected by the evolution process of the dislocation density.

As shown in Eq. (6), when $\varepsilon_0 \leq \varepsilon_i \leq \varepsilon_c$ and k_{2i} is a constant, Eq. (7) can be used to describe the stress σ_{rec} of pure copper DRV:

$$\sigma_{rec} = \sigma_{sat} - (\sigma_{sat} - \sigma_0) \exp\left(-\frac{k_2}{2} (\varepsilon - \varepsilon_0)\right), \quad (7)$$

where σ_0 and ε_0 are the yield stress and its corresponding yield strain, respectively, ε_c is the critical strain of DRX, k_2 is a constant, which can be easily obtained from the linear relationship of $\ln \frac{\sigma_{sat} - \sigma_{rec}}{\sigma_{sat} - \sigma_0}$ and $\varepsilon_i - \varepsilon_0$. When $\varepsilon_c \leq \varepsilon_i \leq \varepsilon_{ss}$, the DRX stress σ_{drx} is expressed as [16]:

$$\sigma_{drx} = \sigma_{rec} - (\sigma_{sat} - \sigma_{ss}) \left\{ 1 - \exp\left[-k_3 \left(\frac{\varepsilon - \varepsilon_c}{\varepsilon_p}\right)^n\right]\right\}, \quad (8)$$

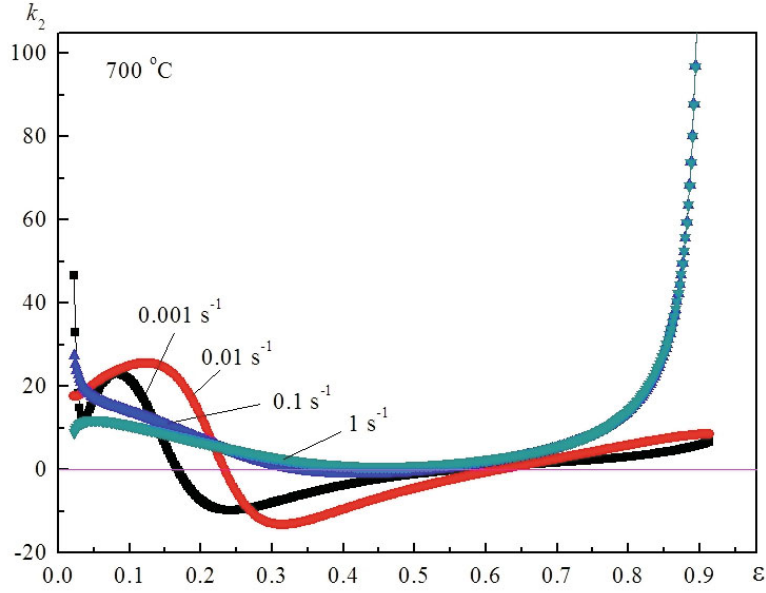


Fig. 2. Evolution of the coefficient k_2 with strain ε under different strain rates at 700°C.

where σ_{ss} is the steady state stress, ε_p is the peak strain, n is the Avrami's power, and k_3 is a constant. According to Eq. (8), a linear relationship of $\ln(-\ln(1 - X_{drx}))$ and $\ln \frac{\varepsilon - \varepsilon_c}{\varepsilon_p}$ is easily obtained, and n and k_3

values are obtained by the fitting calculation, where X_{drx} is the DRX fraction. The DRV stress σ_{rec} and DRX stress σ_{drx} are calculated with Eqs. (7) and (8). The calculated stress-strain curve is consistent with the experimental stress-strain curve without considering SWH, indicating that Eqs. (7) and (8) can reflect the stress-strain rules of pure copper DRV and DRX when the strain is smaller than the steady-state strain.

Figure 3 shows curves of calculated $(\rho - \rho_c)/\rho_c$ and ε . From DRX to DRX steady state, the curve rises, indicating that the dislocation density increases, and then drops, indicating that DRX consumes a large amount of dislocation. In the DRX deformation process of pure copper, when the strain increases, $(\rho - \rho_c)/\rho_c$ value is basically larger than 0, indicating that the dislocation density is higher than the critical value (ρ_c). The high-temperature compression deformation process of pure copper is dominated by the continuous dynamic recrystallization (CDRX) deformation mechanism. In the curves corresponding to the strain rates of 0.001 and 0.01 s^{-1} , the $(\rho - \rho_c)/\rho_c$ value under the DRX steady state is close to 0, indicating that the critical stress σ_c can be replaced by the steady-state stress σ_{ss} . With critical stress and steady-state stress exponents, $n = \partial(\ln \dot{\varepsilon})/\partial(\ln \sigma)$, the corresponding values at 700°C are 6.4 and 5.9, respectively. The same method can be used to calculate stress exponents at other temperatures. Table 1 lists the steady-state stress exponents obtained in previous studies and calculated in this study. The stress exponents remain constant and are close to 6 [17], being insensitive to the processing parameters.

As shown in Fig. 4, under a strain rate of 0.001 s^{-1} , the corresponding X_{drx}/ε value is maximum. The inner deformation energy provides the thermodynamic driving force for DRX nuclei, which is firstly formed at the grain boundary. With an increase in strain, the size of the recrystallized grain increases. The lower strain rate allows the atoms to be sufficiently diffused, and the DRX nuclei grow into recrystallized grains by absorbing the initial microstructure into dynamic recrystallized grains. The recrystallized grains are also easily coarsened. It can be found from Fig. 4 that, under the strain rates of 0.001 and 0.01 s^{-1} , the dynamic recrystallization volume fraction is higher than 99% when the strain reaches steady-state strain. Therefore, it is approximately regarded as an occurrence of a complete dynamic recrystallization process.

After the initiation of DRX, the X_{drx}/ε value corresponding to strain rate 1 s^{-1} increases fastest, and its X_{drx}/ε value is higher than X_{drx}/ε values corresponding to strain rates of 0.01 and 0.1 s^{-1} , indicating that higher

TABLE 1. Steady-State Stress Exponents for the Hot Processing of Pure Copper

Temperature (°C)	Stress exponent	Source of data
260	6.1	[17]
371	5.6	[17]
482	5.4	[17]
600	6.0	This study
700	5.9	This study
750	6.1	This study
800	6.2	This study
850	5.7	This study
900	5.5	This study

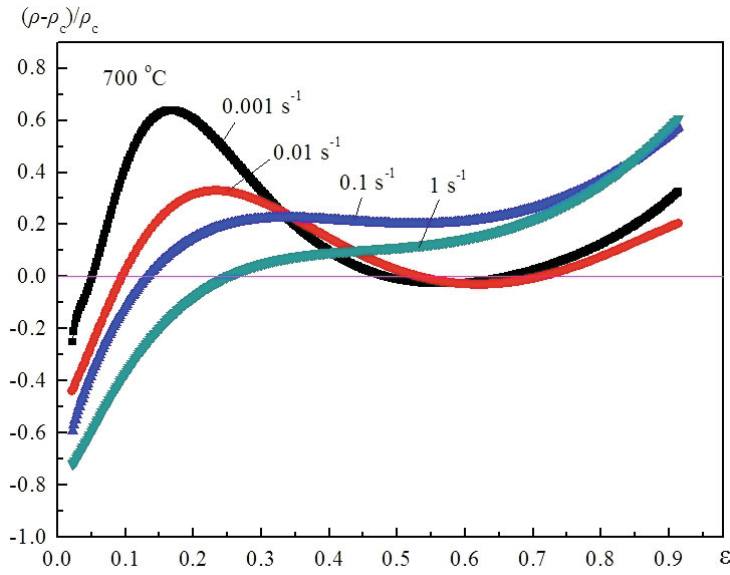


Fig. 3. Curves of $(\rho - \rho_c) / \rho_c$ as a function of ε under different strain rates at 700°C.

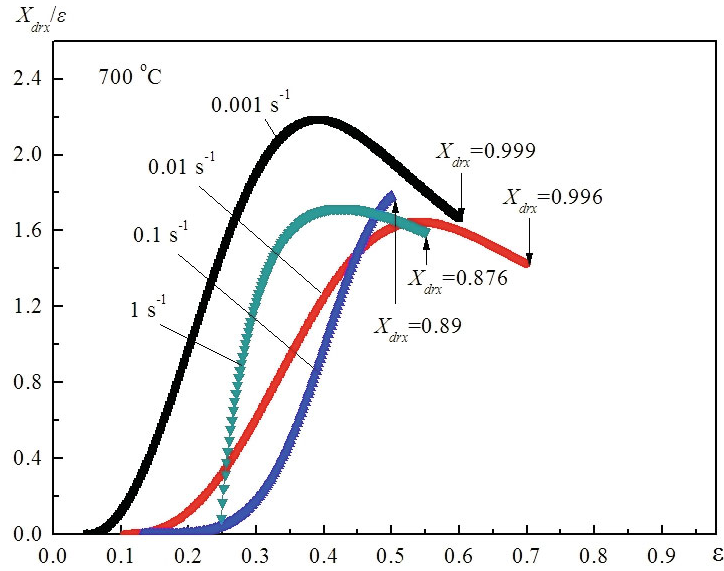


Fig. 4. Curves of X_{drex} / ε as a function of ε at 700°C.

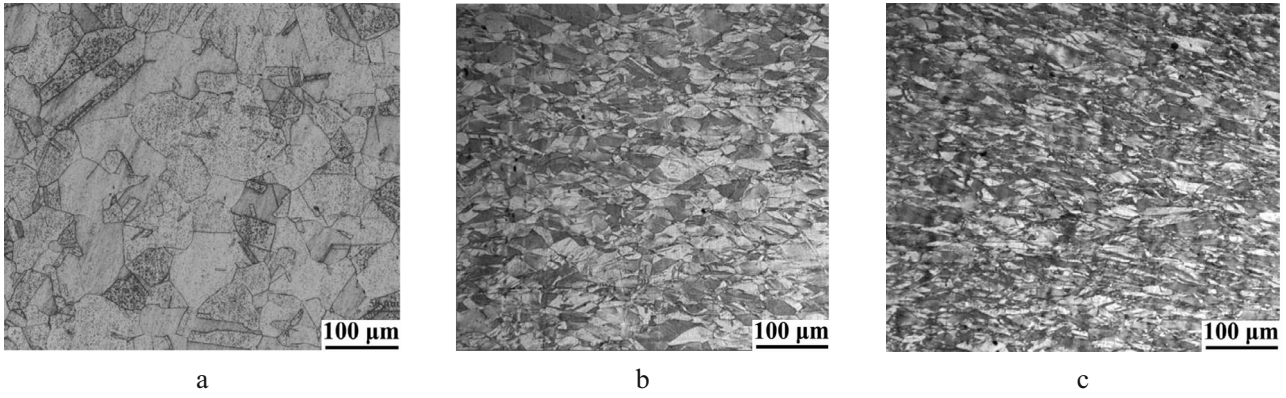


Fig. 5. Optical microstructures of pure copper under different conditions: (a) initial microstructure; (b) 700°C, 0.01 s⁻¹; (c) 600°C, 1 s⁻¹.

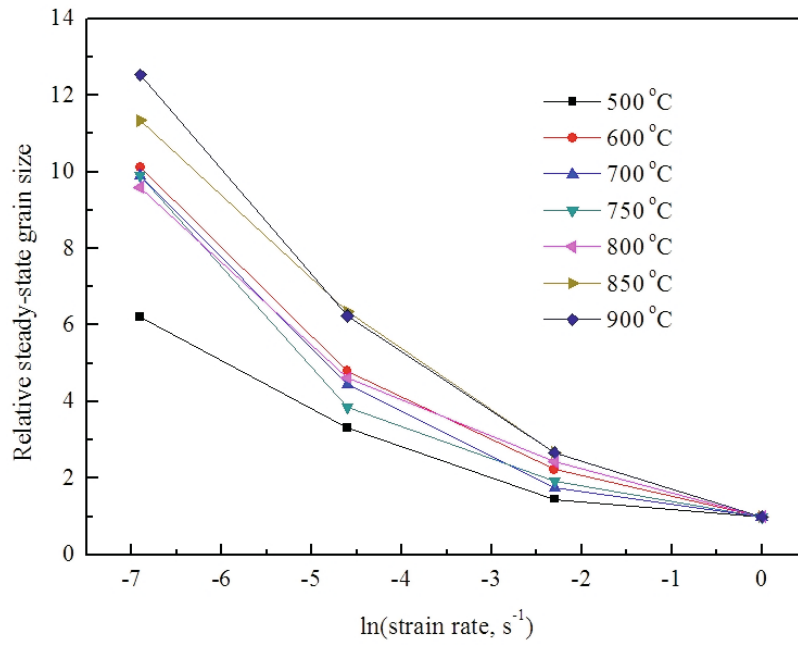


Fig. 6. Relationship between the relative steady-state grain size and strain rate.

the strain rate, the easier the nucleation process of the recrystallized grain, even if the DRX fraction is smaller. Many small DRX grains appear around initial coarse grains. With an increase in strain, the average size of recrystallized grains and the DRX fraction increase. Furthermore, in a small range of strain, it promotes the recrystallized grains to grow rapidly.

Figure 5 is a typical optical microstructure of pure copper. The initial microstructure (Fig. 5a) is basically replaced by the DRX grain microstructure (Fig. 5b). Figure 5c shows the deformed microstructure with the decline in temperature and rise of strain rate; the grain size of dynamic recrystallization is relatively small but the distribution of its grain size is comparatively non-uniform. The stable size of recrystallized grain is not related to the initial grain size in the equality $\sigma_{ss}^2 D_s = \eta^2 \mu^2 b$ [18], where D_s denotes the DRX steady-state grain size and η represents a constant.

In Fig. 6, the DRX steady-state grain size corresponding to the strain rate 1 s⁻¹ is set as a reference value of 1, and the variation patterns of steady-state grain size and logarithmic strain rate are calculated. The relative steady-state grain size increases with the decrease in the strain rate. The higher the temperature, the more obvious the

increase of the steady-state grain size. In other words, with a decrease in the deformation temperature, the strain rate increases, thus resulting in a smaller DRX steady-state grain size.

Conclusions. A modified K–M model was established to explore the evolution of dislocation density of pure copper under high-temperature compression deformation. The relationships between the model parameters (WH coefficient, DRV coefficient, and DRX coefficient) and deformation conditions (deformation temperature, strain rate, and strain) were established. The calculated yield stress curves under different conditions were consistent with the experimental results.

The high-temperature compressive deformation of pure copper was dominated by CDRX deformation mechanism. The critical stress and steady-state stress exponents were basically close to six, being insensitive to the processing parameters. The strain and strain rate had a significant effect on the DRX grain size. With a decrease in temperature and increase in strain rate, DRX steady-state grain sizes were reduced.

Acknowledgments. This research was funded by the Chongqing Research Program of Basic Research and Frontier Technology, China (No. cstc2015jcyjBX0115).

REFERENCES

1. M. Shalbafi, R. Roumina, and R. Mahmudi, “Hot deformation of the extruded Mg–10Li–1Zn alloy: Constitutive analysis and processing maps,” *J. Alloy. Compd.*, **696**, 1269–1277 (2017).
2. P. W. Li, H. Z. Li, L. Huang, et al., “Characterization of hot deformation behavior of AA2014 forging aluminum alloy using processing map,” *T. Nonferr. Metal. Soc.*, **27**, 1677–1688 (2017).
3. Y. T. Wu, Y. C. Liu, C. Li, et al., “Deformation behavior and processing maps of Ni₃Al-based superalloy during isothermal hot compression,” *J. Alloy. Compd.*, **712**, 687–695 (2017).
4. L. Zhang, Q. D. Wang, G. P. Liu, et al., “Effect of SiC particles and the particulate size on the hot deformation and processing map of AZ91 magnesium matrix composites,” *Mater. Sci. Eng. A*, **707**, 315–324 (2017).
5. K. Arun Babu, S. Mandal, C. N. Athreya, et al., “Hot deformation characteristics and processing map of a phosphorous modified super austenitic stainless steel,” *Mater. Design*, **115**, 262–275 (2017).
6. K. Graetz, C. Miessen, and G. Gottstein, “Analysis of steady-state dynamic recrystallization,” *Acta Mater.*, **67**, 58–66 (2014).
7. C. C. Sun, K. Liu, Z. H. Wang, et al., “Hot deformation behaviors and processing maps of Mg–Zn–Er alloys based on Gleeble–1500 hot compression simulation,” *T. Nonferr. Metal. Soc.*, **26**, 3123–3134 (2016).
8. B. Li, Q. L. Pan, and Z. M. Yin, “Characterization of hot deformation behavior of as-homogenized Al–Cu–Li–Sc–Zr alloy using processing maps,” *Mater. Sci. Eng. A*, **614**, 199–206 (2014).
9. H. Matsumoto and V. Velay, “Mesoscale modeling of dynamic recrystallization behavior, grain size evolution, dislocation density, processing map characteristic, and room temperature strength of Ti-6Al-4V alloy forged in the ($\alpha + \beta$) region,” *J. Alloy. Compd.*, **708**, 404–413 (2017).
10. C. Q. Huang, J. Deng, S. X. Wang, et al., “A physical-based constitutive model to describe the strain-hardening and dynamic recovery behaviors of 5754 aluminum alloy,” *Mater. Sci. Eng. A*, **699**, 106–113 (2017).
11. H. Riedel and J. Svoboda, “A model for strain hardening, recovery, recrystallization and grain growth with applications to forming processes of nickel base alloys,” *Mater. Sci. Eng. A*, **665**, 175–183 (2016).
12. K. Huang and R. E. Logé, “A review of dynamic recrystallization phenomena in metallic materials,” *Mater. Design*, **111**, 548–574 (2016).
13. M. Bacca, D. R. Hayhurst, and R. M. McMeeking, “Continuous dynamic recrystallization during severe plastic deformation,” *Mech. Mater.*, **90**, 148–156 (2015).
14. M. Zouari, N. Bozzolo, and R. E. Loge, “Mean field modeling of dynamic and post-dynamic recrystallization during hot deformation of Inconel 718 in the absence of δ phase particles,” *Mater. Sci. Eng. A*, **655**, 408–424 (2016).

15. L. Maire, B. Scholtes, C. Moussa, et al., "Modeling of dynamic and post-dynamic recrystallization by coupling a full field approach to phenomenological laws," *Mater. Design*, **133**, 498–519 (2017).
16. Z. P. Wan, Y. Sun, L. X. Hu, and H. Yu, "Experimental study and numerical simulation of dynamic recrystallization behavior of TiAl-based alloy," *Mater. Design*, **122**, 11–20 (2017).
17. H. Q. Liang, H. Z. Guo, K. Tan, et al., "Correlation between grain size and flow stress during steady-state dynamic recrystallization," *Mater. Sci. Eng. A*, **638**, 357–362 (2015).
18. Y. H. Liu, Z. K. Yao, Y. Q. Ning, et al., "Effect of deformation temperature and strain rate on dynamic recrystallized grain size of a powder metallurgical nickel-based superalloy," *J. Alloy. Compd.*, **691**, 554–563 (2017).